15 Surface Physics

T. Greber, M. Hengsberger, J. H. Dil, F. Matsui, P. Krüger, R. Westerström, L. Castiglioni, H. Cun, B. Slomski, S. Roth, A. Hemmi, G. Landolt, M. Greif, R. Stania, C. Bernard, L. H. de Lima, S. Muff, A. Schuler, F. Dahinden, R. Rüttimann, T. Kälin, J. Osterwalder

The group investigates surface and interface phenomena at the atomic level. For this purpose the surface physics laboratory is well equipped for the preparation and characterization of clean single-crystalline surfaces, metal and molecular monolayer films, as well as covalently bonded single layers, using a wide variety of experimental techniques. In addition to a well equiped laboratory at UZH-Irchel, we currently operate a custom-built end station for spin- and angle-resolved photoemission spectroscopy (SARPES) at the nearby Swiss Light Source (SLS), and we take an active role in the construction and commissioning of the new SLS beamline PEARL (Photo-Emission and Atomic Resolution Laboratory). Moreover, within the NCCR 'Molecular Ultrafast Science and Technology' (MUST), our group has built and commissioned a compact and mobile angle-resolved photoemission instrument, which is currently taking data at the attosecond laser facility in the laboratory of U. Keller at ETHZ[1].

The research carried out during the report period can be grouped into four topics:

- Monolayer films of hexagonal boron nitride (*h*-BN) and graphene on metal surfaces

  Over the last several years the group has built up a considerable expertise in the growth and characterization of sp^2-bonded monolayers on transition metal surfaces. On the one hand, our interest is fueled by the chemical functionality of the adlayers: on Rh(111) and Ru(0001) surfaces, the large lattice misfit induces strongly corrugated sp^2 layers that exhibit also a corrugation in the electrostatic potential landscape that can be exploited for templating molecular adsorbates [2–5]. As a new feature, we could show in this last year that this templating functionality applies also to species intercalated between the sp^2 layer and the metal substrate, induced by gentle ion implantation (see Section 15.1).

  A second line of research is directed towards the synthesis of epitaxial layers of graphene and *h*-BN with a view on future electronic devices based on graphene. Due to its insulating properties and similar crystal structure and lattice constant, *h*-BN appears to be the ideal 'gate oxide'. We have succeeded in growing single-layer graphene on top of single-layer *h*-BN on Cu(111). The two layers are well aligned, but each one maintains its own lattice constant. This leads to the observation of a well defined moiré pattern in scanning tunneling microscopy images, and to the effective decoupling from the substrate of the electrons in the graphene layer (paper submitted).

  Within a Sinergia project of the Swiss National Science Foundation we have built up a growth chamber for handling wafer-size samples, where *h*-BN or graphene films can be grown on four-inch Si(111) wafers covered with monocrystalline Rh(111) films. The chamber is placed in a dedicated clean-room, which enables us to process these samples in a dust-free environment. We are currently working on peel-off methods for producing free-standing mono- or multilayer films of graphene or h-BN on the centimeter scale.

- Molecular adsorbates and molecular monolayers

  One focus here is on endofullerenes that can be viewed as spin shuttles. Samples of $DySc_2@C_{80}$ molecules, obtained from L. Dunsch of the IWF Dresden, show long spin relaxation times at a temperature of 2K [6]. These studies have been extended to other rare earth-nitride cluster endofullerenes, using SQUID and x-ray magnetic circular dichroism measurements.

  An important aspect in designing functionalities in molecular layers is the structure-function relationship. This pertains to magnetic, catalytic and photochemical properties of such layers. Within the NCCR MUST, we are therefore developing the method of ultra-violet photoelectron diffraction for measuring the structure of adsorbed molecules. A study of a monolayer of Sn-phthalocyanine on Ag(111) demonstrates the structural sensitivity of the method (see Section 15.3). In combination with pump-probe experiments using high-harmonic laser pulses, we hope to be able to follow the structural dynamics of adsorbed molecules upon photo-excitation.

- Spin-orbit effects at surfaces

  Our spin-resolved photoemission chamber

(COPHEE) at the SLS has continued to be in high demand as a general user instrument due to its unique performance. The investigations of the Rashba effect in ultrathin Pb films on Si(111) were completed (PhD thesis of B. Slomski), addressing also combined effects of spin-orbit coupling and hybridization between different quantum well states, and their consequences for the spin texture in momentum space. The studies of materials with non-centrosymmetric structure that show a pronounced spin splitting also in bulk electronic states (see Section 15.2) were extended to include also BiTeCl. In collaboration with the group of A. Schilling, the ARPES experiments of the topological insulators of composition $GeBi_{4-x}Sb_xTe_7$ were completed.

- Ultrafast processes at surfaces
With the MUST photoemission spectrometer attached to the attoline in the group of U. Keller, first traces of sub-femtosecond dynamics have been recorded. In particular, RABBITT (Reconstruction of Attosecond Beating By Interference of Two-photon Transitions) traces could be taken for the first time from a solid surface, and concurrently also from a gas target. In this method, photoelectron spectra are recorded while the surface of an Ag(111) or Au(111) sample is hit by a femtosecond infrared laser pulse and an XUV attosecond pulse train with variable time delay. From such data we hope to gain insight into the dynamical processes involved in electron emission from surfaces. Within two student's projects, two time-resolved optical spectroscopy experiments have been built up in our home laser laboratory: surface second harmonic generation (bachelor thesis, F. Dahinden) and absorption spectroscopy (master thesis, A. Schuler).

[1] See http://www.ulp.ethz.ch/research/Attoline.

[2] S. Berner *et al.*, Angew. Chem. Int. Ed. 46, 5115 (2007).

[3] J. H. Dil *et al.*, Science 319, 1824 (2008).

[4] T. Brugger *et al.*, Phys. Rev. B 79, 045407 (2009).

[5] A. J. Pollard *et al.*, Angew. Chem. Int. Ed. 49, 1794 (2010).

[6] R. Westerström *et al.*, J. Am. Chem. Soc. 134, 9840 (2012).

In the following, three highlights of last year's research are presented in more detail.

15.1 Capturing single argon atoms in boron nitride nanotents

In collaboration with Marcella Iannuzzi, Jürg Hutter, Physikalisch Chemisches Institut, Universität Zürich.

At room temperature, it is very difficult to immobilize single atoms, in particular the least reactive noble gases. Ion implantation into a crystal lattice possesses this capability, but the randomness of the involved processes does not permit much control over their distribution within the solid. However, with the assistance of single layers of hexagonal boron nitride (*h*-BN) or graphene, site-selective immobilizing of atoms at surfaces becomes feasible. The *h*-BN nanomesh [1] is a corrugated single layer with a 3.2 nm honeycomb superstructure formed on a Rh(111) surface [2]. Due to the lattice misfit between *h*-BN and Rh, and the preference of nitrogen to bond on top of Rh, the superstructure features two different bonding areas, the 'pores', where the *h*-BN forms chemical bonds with the substrate, and the 'wires' where the *h*-BN has a pure van der Waals bonding to the substrate. Fig.15.1 shows that after Ar implantation, the nanomesh can trap individual argon atoms at room temperature at distinct subsurface sites to form "nanotents".

For Ar implantation, a kinetic energy window (about 20-60 eV) has been identified where the argon ions can penetrate the *h*-BN layer but not enter the Rh lattice. Scanning tunneling microscopy and photoemission data show the presence of argon atoms at two distinct sites (wire crossing sites WXA and WXB in Fig. 15.2B) within the nanomesh unit cell. Fig. 15.2A shows Ar

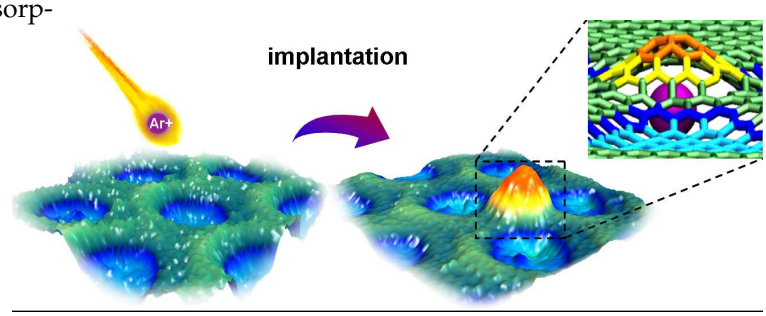

FIG. 15.1 – Nanotent formation by Ar ion implantation (the orange peak) beneath a corrugated monolayer of hexagonal boron nitride. 3D rendered scanning tunneling microscopy images demonstrate one Ar atom implanted beneath the *h*-BN monolayer at a wire crossing site. The purple sphere represents the Ar atom. The *h*-BN wire- and pore- regions are indicated with green and blue color, respectively. The image in the upper right corner is the simulated 3D view of an Ar nanotent.

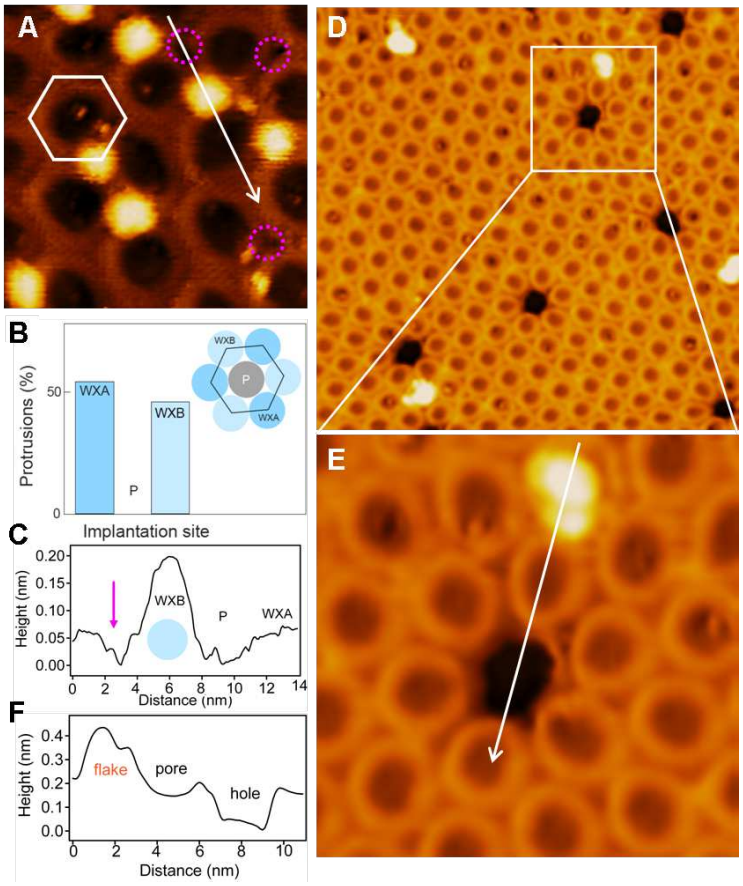

FIG. 15.2 –
Ar implantation and "can-opener" effect.
(A) Atomic-resolution STM image demonstrating Ar implantation beneath the *h*-BN wires (11.4×11.4 nm^2, U = -1.10 V, I = 0.10 nA). The bright protrusions are caused by implanted Ar, and the pink circles indicate vacancy defects generated by the Ar penetration. The hexagon represents the honeycomb supercell, also shown in the inset of (B).
(B) Statistics illustrates the selectivity of the process: Ar stops at two distinct sites beneath nanomesh wire crossings (WXA and WXB), but not in the pores (P).
(C) Cross section along the line in (A) with salient features indicated.
(D) STM image (46×46 nm^2) shows 2 nm holes at pore sites after annealing to 900 K.
(E) High-resolution image (14×14 nm^2, U = -1.10 V, I = 0.50 nA) showing a hole and a flake.
(F) Cross-sectional profile along the line in (E), showing the height difference between the flake and the hole.

atoms implanted beneath the *h*-BN wires as bright protrusions with a large footprint. The two configurations are confirmed by density functional theory calculations - they are metastable. Remarkably, these "nanotents" are predicted to capture up to six Ar atoms, and to be stable in air.

Annealing of implanted structures to 900 K induces the formation of highly regular holes of 2 nm diameter in the *h*-BN layer, with flakes of the same size found near the holes on the surface (Fig. 15.2D-F) [3]. We propose that this "can-opener" effect is due to vacancy defects, generated during the penetration of the Ar ions through the *h*-BN lattice, and their propagation along the rim of a nanomesh pore where the *h*-BN lattice is highly bent. The implantation effects are robust and quite general: they are also observed in graphene on ruthenium and for neon atoms.

[1] M.Corso *et al.*, Science 303, 217 (2004).
[2] S. Berner *et al.*, Angew. Chem. Int. Ed. 46, 5115 (2007).
[3] H. Y. Cun *et al.*, Nano Lett., DOI:10.1021/nl400449y (2013).

15.2 Disentangling surface and bulk Rashba effects in BiTeI

In collaboration with Evgueni V. Chulkov, Departamento de Fisica de Materiales, Donostia International Physics Center, 20080 San Sebastian, Spain; Vladimir N. Strocov, Swiss Light Source, Paul Scherrer Institut, 5232 Villigen, Switzerland; Imamaddin R. Amiraslanov, Physics Institute, Azerbaijan National Academy of Science, AZ1143 Baku, Azerbaijan.

In non-magnetic materials the time-reversal symmetry implies that the electronic band structure is inversion symmetric with respect to the origin in momentum-space. If the material is also inversion symmetric in real space, Kramers theorem applies, which states that all the electronic states in a crystal are spin-degenerate under these conditions, even in the presence of spin-orbit interaction (SOI). An important branch of research in *spintronics* is the hunt for materials in which this Kramers degeneracy is lifted, because they would support the production and the control of spin currents and to eventually realize spin-based logical devices.

The two ingredients for the occurrence of spin-split states in non-magnetic materials are a strong SOI and a broken inversion symmetry. At crystal boundaries, i.e. at surfaces or interfaces, the inversion symmetry is naturally absent and the so-called Rashba effect [1] can oc-

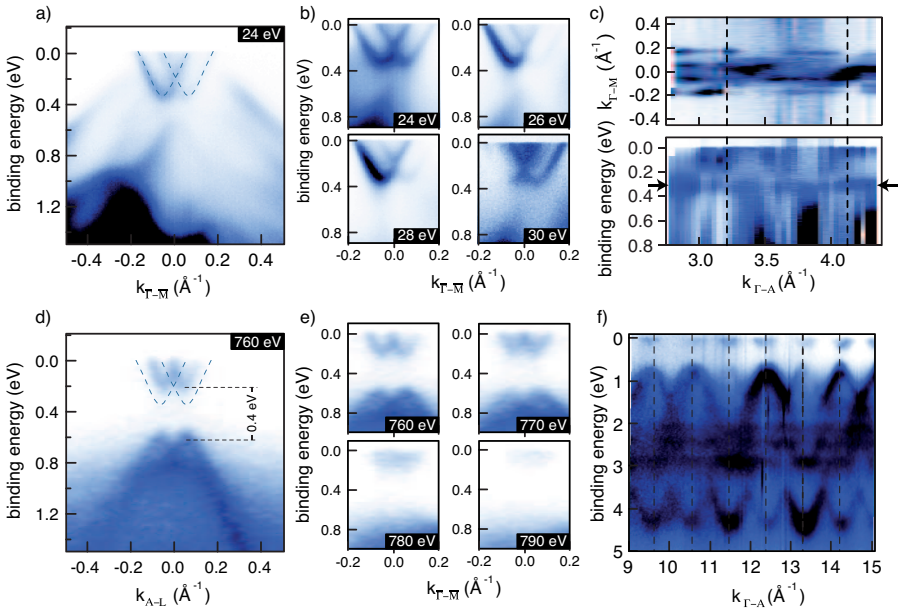

FIG. 15.3 –
Bulk and surface states of BiTeI.
(a) Ultra-violet ARPES band map revealing the presence of surface states.
(b-c) Their two-dimensional character is confirmed by photon energy dependent ARPES.
(d) Soft X-ray ARPES band map showing the large Rashba spin splitting of the bulk bands.
(e-f) Photon energy dependent band maps show strong dispersion and confirm the three-dimensional character of the bulk states.

cur, where the SOI leads to a linear-in-k energy splitting of free-electron-like dispersing states.

When magnetism is absent, the electronic *bulk* states can only be non-degenerate if the crystal unit cell itself lacks inversion symmetry. Such a bulk spin splitting is known to occur in noncentrosymmetric zinc blende and wurzite structures [2], though on a fairly small energy scale. Recently, the semiconductor BiTeI was predicted to feature a strong SOI and a large Rashba effect in the bulk bands, i.e. the occurrence of two momentum-split parabolic bands at the band edge [3]. We have performed the first angle-resolved photoemission spectroscopy (ARPES) measurements of the bulk band structure of this material [4].

BiTeI has a hexagonal crystal structure and is built up of alternating layers of bismuth, tellurium, and iodine atoms stacked along the hexagonal axis. The continuous stacking order of the layers of the three atomic species breaks the inversion symmetry.

Because of the broken inversion symmetry and the weaker bonding between the tellurium and iodine layers, an untwinned BiTeI crystal has two different terminations either purely formed of I or Te atoms, depending on the crystal face forming the surface.

Calculations in the framework of the density functional theory (DFT), performed by the group of E.V. Chulkov, predict the existence of two-dimensional surface states on the two possible surfaces. In order to disentangle the surface and the bulk contributions to the electronic structure we performed ARPES measurements in the ultra-violet (UV-ARPES) and the soft x-ray photon energy regime (SX-ARPES). In UV-ARPES, photoemission from the surface states is dominant over bulk state emission, while the latter is emphasized in the more bulk sensitive SX-ARPES.

The UV-ARPES measurements of Fig. 15.3a show the coexistence of both, the spin-split electron-like (Te-termination) and hole-like (I-termination) surface state, indicating surfaces with mixed terminations. The photon energy dependent UV-ARPES measurements in Figs. 15.3b-c exhibit no k_z dispersion (along the sample surface normal) which confirms the two-dimensional character of the observed states. For comparison Fig. 15.3d shows SX-ARPES maps of the near-gap bulk valence and conduction bands and confirms the predicted large bulk Rashba effect. The photon energy dependent SX-ARPES measurements in Fig. 15.3e-f exhibit clear k_z dispersion, commensurate with the bulk Brillouin zone, and confirm the three-dimensional bulk character of the measured states.

The soft X-ray photon energy scan of the bulk Fermi surface in Fig. 15.4a is in excellent agreement with the DFT calculations (Fig. 15.4b) and completes the picture of the complex bulk Fermi surface. Figure 15.4c illustrates the three-dimensional Fermi surface, which takes the shape of a spindle-torus distorted according to the crystal symmetry. When the chemical potential is tuned below the degeneracy point at the A point, the Fermi surface undergoes a topological transition to a regular torus. Such a toroidal, single-spin Fermi surface has unique properties and may open a pathway for the realization of exotic physical phenomena.

[1] Y. A. Bychkov and E. I. Rashba, J. Phys. C: Solid State Physics, 17, 6039 (1984).
[2] G. Dresselhaus, Phys. Rev. 100, 580 (1955).
[3] K. Ishizaka, Nature Materials 10, 521 (2011).
[4] G. Landolt, Phys. Rev. Lett. 109, 116403 (2012).

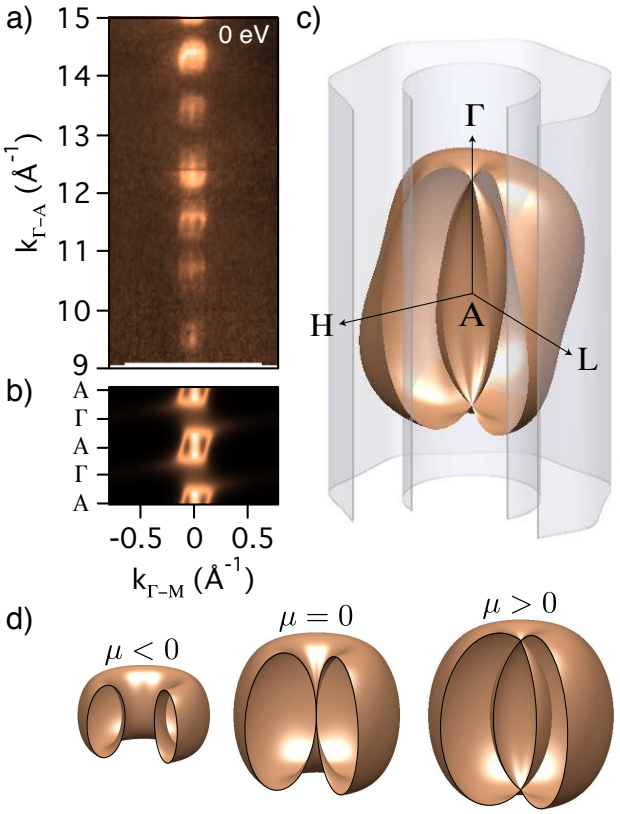

FIG. 15.4 –
(a) Soft X-ray ARPES bulk Fermi surface map.
(b) Bulk Fermi surface calculated by DFT.
(c) Schematic representation of the three-dimensional spindle-torus-like Fermi surface of the bulk states (orange) and the k_z-independent Fermi surface of the electron-like surface state (gray).
(d) Topological transition of the toroidal bulk Fermi surface as a function of the chemical potential.

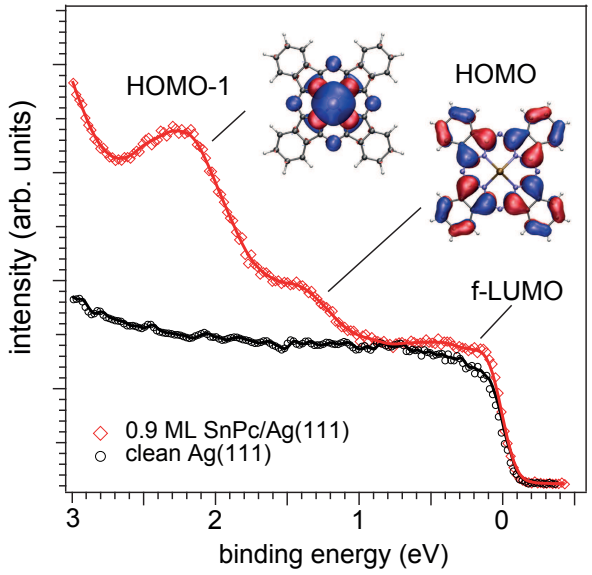

FIG. 15.5 – UPS spectra near the Fermi energy of pristine Ag(111) (black) and 0.9ML SnPc/Ag(111) (red) showing the highest occupied molecular orbital (HOMO) states beside the real-space charge distribution of the corresponding orbitals.

15.3 Photoelectron diffraction from Sn-phthalocyanine

In collaboration with Peter Krüger, Université de Bourgogne, 21078 Dijon, France; Markus Meuwly, University of Basel, 4056 Basel.

In photoemission from solid surfaces the outgoing photoelectron wave is coherently scattered at atoms in the close vicinity of the source atom. The direct and scattered waves generate an interference pattern, which contains information about the coordination of the emitter atom [1] and the spatial extent of the orbital from which the electron is emitted [2, 3]. Excited with EUV light (10-100 eV) this method is termed ultra-violet photoelectron diffraction (UPD), in the case of x-rays XPD. In both experiments, the photoemission intensity at fixed kinetic energy is recorded as function of emission direction. From the photoelectron spectrum the initial state can be chosen as shown in Fig. 15.5.

While UPD offers significant advantages in view of time-resolved measurements over the more established x-ray variant, the interpretation of the data is more difficult due to the higher complexity of the molecular initial states. Therefore, we engaged in a close collaboration with theory groups. The idea is to compute first the atomic and electronic structure for the molecule adsorbed on the surface using DFT, and then the evolution of the molecular state by means of Molecular Mechanics calculations [4]. The computed trajectories serve as input for scattering calculations, which allow the UPD patterns to be simulated and compared to experiments [3].

In order to demonstrate the capabilities of photoelectron diffraction in terms of molecular structure determination and tracking of transient structural changes, we applied XPD and UPD to a rather complex surface system: Sn-phthalocyanine (SnPc) molecules adsorbed on Ag(111) [5]. It was previously shown that SnPc grows layer-by-layer with the molecules lying flat on the Ag(111) surface [6]. At sub-monolayer coverage the adlayer has different structural phases, which are associated with a conformational change of the SnPc molecule. Conformations with the Sn atom on top of the molecular plane (*tin-up*) or with the Sn atom beneath the molecular plane (*tin-down*) were identified. The different geometrical phases can be tuned via temperature changes. The measurements show that the non-planar molecules undergo flattening upon adsorption.

In our experiments, XPD patterns were recorded from the Sn 3*d* core level and compared to single-scattering-cluster (SSC) calculations. The flattening of the molecule could be corroborated, and the azimuthal orientation obtained from XPD was in good agreement with values from scanning tunneling microscopy [9]. In photoemis-

sion [7] and DFT studies [8] it was found that the second highest occupied molecular orbital (HOMO-1) plays an important role in the chemical bonding of molecules and substrate. The HOMO-1 is of mainly p_z-character and is localized at the central Sn atom, as can be seen in the inset of Fig. 15.5. UPD measurements taken from the HOMO-1 are shown in Fig. 15.6. Again, the outcome was compared to SSC calculations and reasonable agreement was found between experiment and theory when the incommensurate ordering and the three rotational domains were taken into account (Fig. 15.6). This is surprising because at low energies multiple scattering is known to strongly influence the interference patterns. The upgrade to multiple scattering calculations for computing the electronic structure *and* the scattering patterns are part of ongoing work.

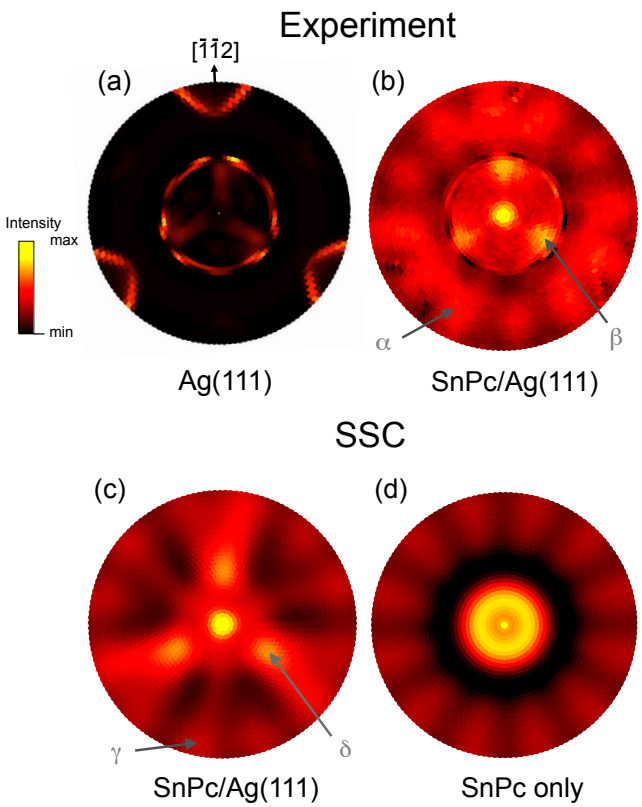

FIG. 15.6 – UPD taken with EUV light (21.2 eV) from the HOMO-1.
(a) Pattern taken from the Ag(111) substrate at the corresponding energy.
(b) Measured UPD pattern from the HOMO-1 at a coverage of 0.9 ML.
(c) SSC calculation of the pattern from a single molecule, averaging over many local registries with the Ag(111) surface due to the incommensurate adsorbate layer, and over the three rotational domains. Arrows indicate corresponding features.
(d) SSC calculation of the pattern from a single, free-standing molecule, averaged over three rotational domains.

[1] J. Osterwalder *et al.*, Chimia 60 (2006) A795.
[2] P. Puschnig *et al.*, Science 326, 702 (2009).
[3] P. Krüger, F. Da Pieve, and J. Osterwalder, Phys. Rev. B 83 (2011) 115437.
[4] I. Tubert-Brohmann, M. Schmid, and M. Meuwly, J. Chem. Theory Comput. 5 (2009) 530.
[5] M. Greif *et al.*, Phys. Rev. B 87, 085429 (2013).
[6] C. Stadler *et al.*, Nature Phys. 5, 153 (2009).
[7] M. Häming, C. Scheuermann, A. Scholl, F. Reinert, and E. Umbach, J. Elec. Spec. Rel. Phen. 174, 59 (2009).
[8] J. D. Baran and J. A. Larsson,J. Phys. Chem. C 116, 9487 (2012).
[9] M. Toader and M. Hietschold, J. Phys. Chem. C 115, 3099 (2011); *ibid.* 115, 12494 (2011).